

Coupling between CaWO_4 phonons and Er^{3+} dopants

Mikhael T. Sayat,^{1,2,*} Federico Pisani,^{3,*} Hin Lok Chang,⁴ Yaroslav Zhumagulov,⁵ Kirrily C. Rule,⁶ Tom Fennell,⁷ Jakob Nunnendorf,⁴ Chee Kwan Gan,⁸ Oleg V. Yazyev,⁵ Ping Koy Lam,^{1,2,9} and Jian-Rui Soh^{1,2,9}

¹Quantum Innovation Centre (Q.InC), Agency for Science, Technology and Research (A*STAR),

²Fusionopolis Way, Innovis #08-03, Singapore 138634, Singapore

²Centre for Quantum Technologies, National University of Singapore, 3 Science Drive 2, Singapore 117543, Singapore

³Institute of Physics, École Polytechnique Fédérale de Lausanne (EPFL), CH-1015 Lausanne, Switzerland

⁴National University of Singapore, Science Drive 3, Singapore 117551, Singapore

⁵Institute of Physics, École Polytechnique Fédérale de Lausanne, CH-1015 Lausanne, Switzerland

⁶Australian Center for Neutron Scattering, Australian Nuclear Science and Technology Organization, NSW, 2232, Australia

⁷Paul Scherrer Institut Center for Neutron and Muon Sciences, 5232 Villigen PSI, Switzerland

⁸Institute of High Performance Computing (IHPC), Agency for Science,

Technology and Research (A*STAR), 1 Fusionopolis Way, #16-16 Connexis, Singapore 138632

⁹Department of Quantum Science and Technology, Research School of Physics,

Australian National University, Canberra, ACT, 2601, Australia

(Dated: February 10, 2026)

We investigate the lattice dynamics of CaWO_4 , a promising host crystal for erbium-based quantum memories, using inelastic neutron scattering together with density-functional perturbation theory. The measured phonon dispersion along the (100), (001), and (101) reciprocal space direction reveals phonon bands extending up to 130 meV, with a gap between 60 and 80 meV, in good agreement with our calculations. From a symmetry analysis of the phonon eigenmodes, we identify eight Raman-active modes that can couple directly to the Er^{3+} crystal-field operators, including a low-energy B_g mode at 9.1 meV that is expected to play a dominant role in phonon-assisted spin-lattice relaxation. These results provide a microscopic description of the phonon bath in CaWO_4 and establish a basis for engineering phononic environments to mitigate the loss of stored quantum states and optimize Er-doped CaWO_4 for quantum-memory applications.

I. INTRODUCTION

The realization of large-scale quantum networks relies on the development of efficient and long-lived quantum memories that enable the on-demand storage and retrieval of quantum information. Among the many candidate systems such as single atoms [1], nitrogen vacancy centres [2, 3], warm vapour cells [4, 5], and cold atoms [6], solid-state crystals doped with rare-earth ions have emerged as one of the most promising platforms for scalable quantum memories [7–12]. Rare-earth ion-doped crystals combine the advantages of atomic-like optical transitions with the stability and scalability of solid-state environments, enabling long storage times, high-fidelity retrieval and seamless integration with photonic architectures.

Among the available rare-earth ion dopants, erbium (Er^{3+}) is particularly attractive because its optical transitions ($\sim 1.5\mu\text{m}$) lie within the C-band low-loss window of optical fibers, which enables direct compatibility and ease of integration with existing telecommunication networks [13]. However, Er^{3+} ions possess a large magnetic dipole moment ($J=15/2$) that couples both to other magnetic species and to the lattice vibrations of the host crystal, via the spin-spin and spin-lattice interactions, respectively [14].

The effects of the spin-spin interaction can be mitigated by (i) selecting host crystals with exceptionally low nuclear-spin densities, such as Y_2SiO_5 and CaWO_4 , (ii) operating at zero first-order Zeeman (ZEFOZ) conditions [15–17] or (iii) applying strong magnetic fields [18]. These strategies are aimed at creating a low magnetic-noise environment for the embedded Er^{3+} ions, to extend their coherence times. However, while magnetic noise can be largely suppressed through these approaches, lattice vibrational noise is an intrin-

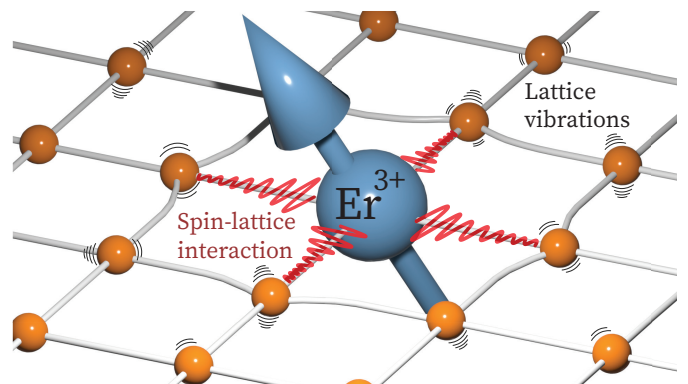


Figure 1. The interaction between the large Er^{3+} magnetic moment and the lattice vibrations (phonons) of the host crystal causes spin-lattice relaxation.

* These authors contributed equally to this work.

sic property of the crystal and remains difficult to eliminate. Phonons that couple to the large magnetic moment of Er^{3+} via the spin-lattice interaction ultimately set an upper bound on how long an excited state can be maintained and therefore on the achievable coherence time.

Spin-lattice relaxation in these rare-earth ion doped systems typically occurs via three main mechanisms: the direct, Raman, and Orbach processes [19, 20]. The Raman and Orbach mechanisms involve two- and three-phonon interactions, respectively, and their rates decrease rapidly with temperature. Hence, they can be effectively suppressed by cooling to cryogenic temperatures [21–23]. In contrast, the direct process, which involves the resonant absorption or emission of a single phonon, persists even at millikelvin temperatures. These residual phonons continue to induce decoherence and ultimately lead to the loss of stored quantum information.

A key step toward mitigating this direct-phonon induced relaxation is to identify the specific phonon modes that couple most strongly to the Er^{3+} crystal-field manifold. Accomplishing this requires a detailed understanding of the complete phonon spectrum of the host crystal. However, previous studies of the lattice vibrations in CaWO_4 have predominately relied on optical (infrared and Raman) spectroscopy, which are intrinsically sensitive only to zone-centre (Γ -point) phonons owing to the short probing wavelength of light [24–33]. Consequently, these techniques provide limited insight into the full phonon dispersion throughout the Brillouin zone. In principle, inelastic neutron scattering (INS) enables the measurement of phonon modes beyond the Γ point.

However, previous INS studies on CaWO_4 by Goel *et al.* [34] were performed on polycrystalline samples, in which the averaging over random crystallite orientations collapses the momentum-transfer information into a one-dimensional phonon density of states (DOS), thereby losing information about the phonon dispersion across the Brillouin zone. Kesavasamy *et al.* [35] succeeded in probing phonons away from the zone center, but their measurements were limited to energies below ~ 37 meV, thus excluding the high-energy optical branches. Therefore, a comprehensive experimental mapping of the phonon spectrum of CaWO_4 spanning both low and high energy regimes across the full Brillouin zone is still lacking. Such measurements are essential for identifying phonon modes that couple most strongly to the Er^{3+} crystal-field levels, which underpin spin-lattice relaxation and the loss of stored quantum information.

In this work, the phonon spectra of the CaWO_4 host crystal is mapped computationally, through density functional perturbation theory, and experimentally, via inelastic neutron scattering. Next, using symmetry analysis, we identified the lattice vibrational modes that couple most strongly to the crystal electric field manifold of Er^{3+} ions. We use this approach to identify the modes that we would target for phonon engineering to generate a phonon band gap [36, 37]. This reduces lattice-induced relaxation of the stored photons and provide

a pathway to develop scalable $\text{Er}^{3+}:\text{CaWO}_4$ quantum memories with long storage and coherence times.

II. METHODS

Single crystals of CaWO_4 grown by the floating-zone method were obtained from SurfaceNet GmBH. The quality and structure of the CaWO_4 single crystals were checked with laboratory x-rays ($\text{Cu, } K_\alpha$) on a 6-circle diffractometer (Bruker). A small piece, approximately 1 mm in diameter, cleaved from the single crystal used for INS measurements, was used for this quality check. In particular, more than 200 unique reflections were measured to determine space group symmetry and crystal cell parameters of CaWO_4 .

To ascertain the lattice dynamics of CaWO_4 , we performed density functional perturbation theory (DFPT) calculations of the phonon dispersion using QUANTUM ESPRESSO. Norm-conserving pseudopotentials [38] within the local density approximation (LDA) were employed. The wavefunctions were expanded in a plane-wave basis with a kinetic-energy cutoff of 80 Ry. The electronic Brillouin zone was sampled using a Γ -centered Monkhorst-Pack \mathbf{k} -point mesh of $8 \times 8 \times 8$ [39]. Phonon properties were computed within density-functional perturbation theory on a uniform $6 \times 6 \times 6$ grid of phonon wavevectors (\mathbf{q} points). The acoustic sum rule was enforced at Γ prior to interpolation.

In order to experimentally verify our DFPT calculations of the phonon spectrum, we performed inelastic neutron scattering measurements on the EIGER triple-axis spectrometer (TAS) at SINQ (PSI), Switzerland [40] and the Taipan TAS at the Australian Centre for Neutron Scattering at the Australian Nuclear Science and Technology Organisation (ANSTO) [41, 42]. The EIGER and Taipan instruments, respectively, were used to map the low (2–60 meV) and high (80–130 meV) energy phonon modes. These energy ranges were selected based on the phonon DOS measurements on CaWO_4 report by Goel *et al.* [34], which found phonon in the energy ranges between 2–60 meV and 80–130 meV.

Phonon spectra were collected by performing energy scans, at various fixed momentum transfers, $\mathbf{q} = \mathbf{k}_f - \mathbf{k}_i$, along high-symmetry reciprocal space directions in the $(h, 0, l)$ scattering plane [Fig. 2b]. These energy scans were performed by fixing the outgoing wavevector at $\mathbf{k}_f = 2.66 \text{ \AA}^{-1}$ ($E_f = 14.86$ meV) and varying the incident neutron wavevector (\mathbf{k}_i) using an incident beam monochromator to achieve the desired energy (ΔE). For low energy transfers ($\Delta E \leq 60$ meV) on the EIGER instrument a pyrolytic graphite (PG) (002) double-focusing monochromator was used, and for high energies ($\Delta E \geq 80$ meV) on the Taipan instrument, a Cu (200) vertically focusing monochromator was used with open-40°-40°-open collimation. In both instruments, a PG (002) analyzer and ^3He tube were used to resolve and detect

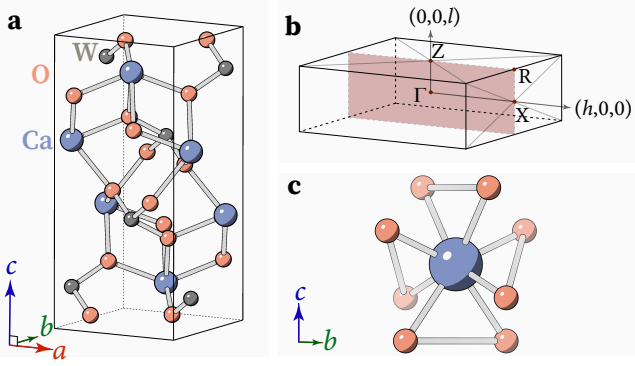


Figure 2. **a** The tetragonal unit cell of CaWO_4 is described by the $I4_1/a$ space group. **b** The corresponding Brillouin zone of CaWO_4 with the $(h, 0, l)$ scattering plane depicted in red. The labels are the high symmetry points. **c** Erbium dopants are coordinated by eight oxygen ligands in a ErO_8 polyhedron.

the scattered neutrons, respectively.

To mitigate the weak neutron cross-section of phonons, large single crystals of CaWO_4 with typical dimensions of $2 \times 2 \times 1 \text{ cm}^3$ were used for both INS experiments. The INS experiments were conducted at $T=200 \text{ K}$. Prior to the inelastic scattering measurements, the CaWO_4 single crystals were oriented on the ORION single-crystal diffractometer (SINQ, PSI). The alignment was performed such that the crystallographic a and c axes lay within the horizontal scattering plane, thereby allowing access to phonon excitations in the $(h, 0, l)$ reciprocal-lattice plane [Fig. 2]. Because CaWO_4 crystallizes in the tetragonal $I4_1/a$ space group, the a and b axes are symmetry equivalent. Consequently, restricting the measurements to the $a-c$ plane captures the essential lattice dynamics without loss of generality.

III. RESULTS

A. Crystal structure

All of the observed x-ray diffraction peaks can be indexed by the tetragonal $I4_1/a$ space group. The refined lattice parameters at room temperature of $a=b=5.2387(5) \text{ \AA}$ and $c=11.3780(10) \text{ \AA}$, are in good agreement with previously reported values [43–45]. The left panel of Fig. 3 plots the measured x-ray diffraction peaks within the $(h, 0, l)$ scattering plane. Indeed, the measured intensity distribution and pattern are in excellent agreement with the calculated reciprocal space map, shown on the right panel of Fig. 3. Along the $(0, 0, l)$ direction, only reflections with $l=4n$ are observed, consistent with the 4_1 screw axis along c , while along $(h, 0, 0)$ only reflections with even h appear. More generally, the body-centering condition imposes $h+l=2n$ for allowed reflections.

These extinction rules demarcate the first Brillouin

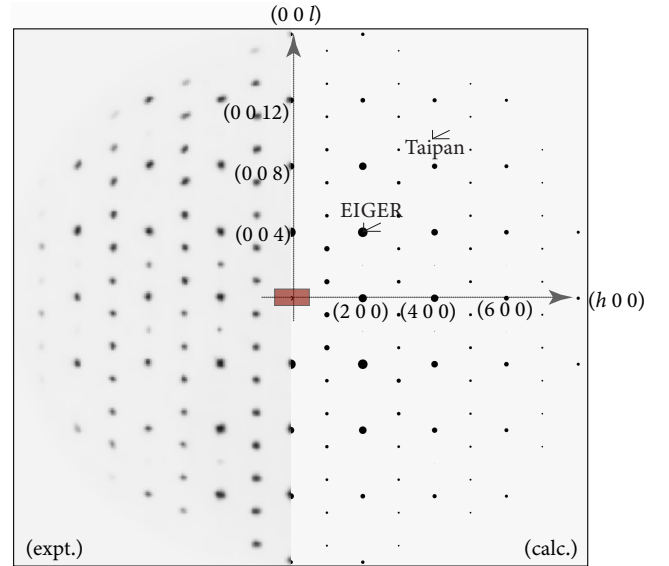


Figure 3. The comparison between the experimental (left) and calculated (right) reciprocal space map of CaWO_4 in the $(h, 0, l)$ scattering plane obtained with single crystal x-ray diffraction. The corresponding first Brillouin zone is depicted by the red rectangle, along with the reciprocal space trajectory of the INS experiments on the EIGER and Taipan triple-axis spectrometers.

zone (in red) within the $(h, 0, l)$ plane, as shown in Fig. 3. The corresponding high symmetry point labels are denoted in Fig. 2b, with the zone center at $\Gamma=(0, 0, 0)$ and the vertical and horizontal axis corresponding to $Z=(0, 0, \frac{1}{2})$ and $X=(\frac{1}{2}, 0, 0)$, respectively.

B. Lattice Dynamics

Having established the crystal structure of CaWO_4 , we now investigate its lattice dynamics from our DFPT calculations. Figure 4 plots the calculated phonon dispersion of CaWO_4 (in red) following the $Z-\Gamma-Z|R-\Gamma-R|X-\Gamma-X$ high-symmetry path in the $(h, 0, l)$ reciprocal space plane, as defined in Fig. 2b. The calculations yield a total of 36 phonon branches, consistent with the 12-atom conventional tetragonal unit cell (2 formula units \times 6 atoms per unit \times 3 degrees of freedom).

The calculated dispersion reflects the $I4_1/a$ tetragonal symmetry of the scheelite lattice. The three acoustic modes extend up to approximately 10 meV, followed by a broad manifold of low-energy optical modes spanning 10–58 meV, originating predominantly from vibrations involving the heavier Ca and W atoms. A band gap of roughly 40 meV separates these from the high-energy optical modes located between 98–115 meV, which arise from stiff W-O bond stretching within the WO_4 tetrahedra [26, 46]. The presence of such a gap is a characteristic feature of scheelite-structured materials [47, 48].

To validate the DFPT calculations, the experimentally

measured phonon excitations from our inelastic neutron scattering (INS) experiments are overlaid as blue markers in Fig. 4. Guided by prior INS studies on polycrystalline CaWO_4 [34], we targeted both the low-energy (2-60 meV) and high-energy (80-130 meV) regions of the spectrum. Acoustic and low-lying optical modes were performed on the EIGER spectrometer, while the high-energy optical excitations were accessed using the Taipan spectrometer. The respective zone centers (Γ -point) are located at $(2, 0, 4)$ and $(4, 0, 10)$, to enable the mapping of phonons along the Γ -Z, Γ -X, and Γ -R directions within the $(h, 0, l)$ plane (Figs. 2b and 3).

Overall, we find a good agreement between the measured low-energy (2-60 meV) phonon branches and calculations, confirming the reliability of DFPT in this regime. At higher energies, the measurements exhibit slightly reduced phonon energies compared to the calculated dispersion. This deviation is expected, as the DFPT calculations were performed at 0 K, whereas the INS measurements were acquired at 200 K, where anharmonic effects soften the phonon frequencies. Nevertheless, the measured excitations remain within the predicted spectral range and broadly follow the calculated phonon dispersion.

Our results are also consistent with previous spectroscopic studies. For instance, Goel *et al.* [34] reported a phonon density of states extending up to ~ 130 meV with a pronounced reduction in intensity between ~ 60 -95 meV, consistent with the optical phonon band gap observed here. Similarly, earlier INS measurements along Γ -Z up to ~ 37 meV by Kesavasamy *et al.* [35] agree well with both our DFPT predictions and experimental dispersion in that regime. Furthermore, the comparison of the measured phonon eigenmodes extracted at the Γ -point show excellent correspondence across both low-

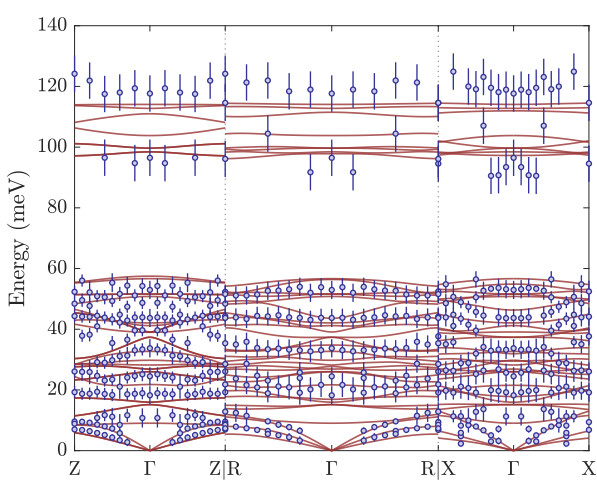


Figure 4. The calculated (red lines) and experimental (blue circles) phonon dispersion of CaWO_4 along the $\text{Z}-\Gamma-\text{Z}|\text{R}-\Gamma-\text{R}|\text{X}-\Gamma-\text{X}$ high-symmetry path.

and high-energy modes, with previously reported Raman and infrared spectroscopy data [Fig. 5].

Taken together, our INS measurements and DFPT calculations establish a robust and comprehensive phonon description of CaWO_4 , and sets the stage for exploring how the lattice vibrations couple to the rare-earth Er^{3+} dopants, which is the focus of the next section.

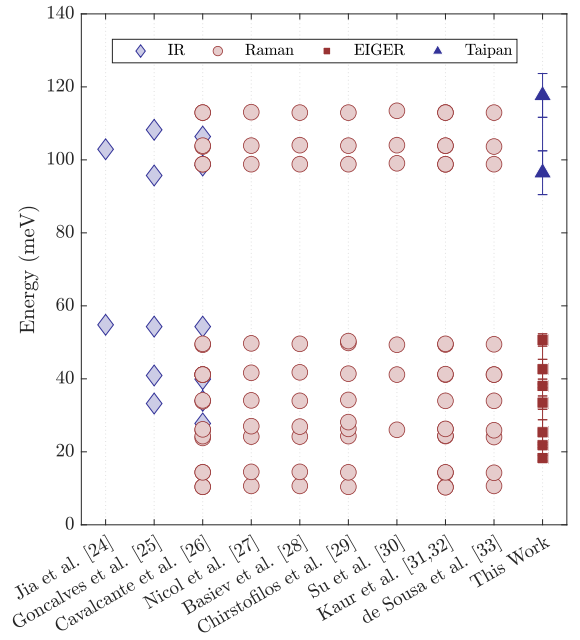


Figure 5. Comparison between previously reported infrared [24-26] and Raman [26-33] active modes and the Γ -point phonon modes measured in this work.

C. Er^{3+} -phonon coupling

We now examine how the Γ -point phonons of CaWO_4 couple to the crystal electric field (CEF) levels of erbium. In CaWO_4 , Er^{3+} occupies the Ca^{2+} site with local S_4 symmetry. As such only terms with $q=0$ and $q=4$ in the Stevens expansion $\hat{H}_{\text{CF}} = \sum_{k,q} B_k^q O_k^q$ are symmetry-allowed, which leads to the following Er^{3+} CEF Hamiltonian,

$$\hat{H}_{\text{CEF}} = B_2^0 O_2^0 + B_4^0 O_4^0 + B_4^4 O_4^4 + B_6^0 O_6^0 + B_6^4 O_6^4. \quad (1)$$

The interaction between the electronic states of Er^{3+} and the phonons of CaWO_4 can be explained by modification of the CEF parameters by the displacement of the surrounding oxygen ligands [Fig. 1c]. Each phonon mode that distorts the ErO_8 coordination polyhedron modifies the crystal-field potential, and modulates the Stevens parameters B_k^q . From a group-theoretical point of view, the effect can be described as the direct product of the irreducible representation (irrep) of a phonon

mode with that of a Stevens operator. Crucially, only those combinations that contain the totally symmetric representation of the site symmetry group produce non-zero matrix elements, and therefore only these phonons contribute directly to crystal-field-phonon coupling.

Formally, the dependence of the crystal-field parameters on the phonon displacement can be written as an expansion,

$$B_k^q(\{Q_\lambda\}) = B_k^q + \sum_\lambda \left(\frac{\partial B_k^q}{\partial Q_\lambda} \right) Q_\lambda + \frac{1}{2} \sum_{\lambda\lambda'} \left(\frac{\partial^2 B_k^q}{\partial Q_\lambda \partial Q_{\lambda'}} \right) Q_\lambda Q_{\lambda'} + \dots, \quad (2)$$

where first term corresponds to the static crystal field, while the second and third terms describe linear and quadratic crystal-field-phonon interactions, respectively. Quantization of the displacement coordinates Q_λ in terms of creation and annihilation operators gives the following crystal-field-phonon coupling Hamiltonian

$$\hat{H}_{\text{cf-ph}} = \sum_{k,q,\lambda} g_{kq,\lambda} O_k^q (a_\lambda + a_\lambda^\dagger) + \sum_{k,q,\lambda\lambda'} h_{kq,\lambda\lambda'} O_k^q (a_\lambda + a_\lambda^\dagger)(a_{\lambda'} + a_{\lambda'}^\dagger) + \dots, \quad (3)$$

where $g_{kq,\lambda}$ and $h_{kq,\lambda\lambda'}$ are coupling constants related to the derivatives of B_k^q with respect to the phonon displacement. The linear term produces one-phonon processes, while the quadratic term allows two-phonon interactions, which can play a role in multiphonon relaxation.

The phonon eigenmodes at the Brillouin-zone center reflect the C_{4h} point group symmetry of the tetragonal scheelite lattice ($I4_1/a$), and can be categorized based on their symmetry. Group-theoretical analysis predicts a set of Raman-active and infrared-active modes. The Raman-active sector comprises $3A_g + 5B_g + 5E_g$, while the infrared-active sector comprises $4A_u + 4E_u$, where E modes are doubly-degenerate. Additional silent $3B_u$ modes and the three acoustic branches complete the spectrum.

Symmetry strongly constrains which phonons participate in crystal-field-phonon scattering process. As we mentioned before, at the S_4 site occupied by Er^{3+} in CaWO_4 , the only Stevens operators that appear in the crystal-field Hamiltonian are O_2^0 , O_4^0 , O_4^4 , O_6^0 , and O_6^4 . The corresponding phonons must have the same irrep. Raman-active A_g modes couple to the axial operators O_k^0 , while B_g modes couple to the fourfold operators O_k^4 . From our DFPT calculations, the relevant B_g modes in CaWO_4 occur at 9.1, 29.8, 42.1, 50.8, and 103.8 meV, respectively, and the A_g modes appear at 28.2, 41.2, and 112.8 meV. The associated $3A_g$ and $5B_g$ eigenmodes are plotted in Fig. 6. Other even-parity modes, such as E_g , do not couple linearly but can contribute through

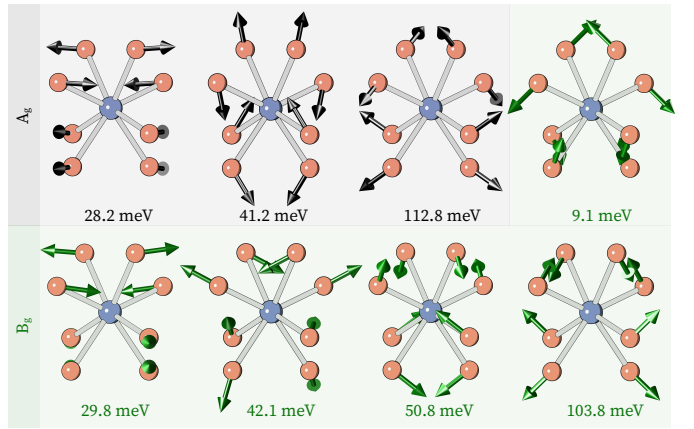


Figure 6. The three A_g and five B_g zone-center phonon eigenmodes which can couple to the Er^{3+} CEF manifold, by symmetry, and the corresponding eigen energies.

quadratic couplings. Odd-parity infrared-active A_u and E_u phonons are excluded from direct linear coupling by inversion symmetry. However, they can become important in higher-order processes and when inversion is locally broken by defects or strain.

IV. DISCUSSION

Mapping the phonon spectrum of CaWO_4 experimentally, is a key step toward identifying which lattice vibrational modes are ultimately responsible for the loss of quantum information stored in rare-earth ions. Further characterisation of CaWO_4 , such as its dielectric properties [49], could be performed to ascertain feasibility in different applications. Beyond quantum-memory applications, CaWO_4 is also of interest as a cryogenic scintillator for rare-event and dark-matter detection, where lattice vibrations play a central role in energy relaxation and signal formation [50–54]. In particular, our inelastic neutron scattering results validate the DFPT-calculated phonon spectrum, which provide a basis for determining which phonon eigenmodes can couple to Er^{3+} dopants, by symmetry. Such a coupling can mediate relaxation and dephasing pathways for stored quantum states, ultimately limiting both the achievable optical storage and coherence time. Even at cryogenic temperatures and in a host with a comparatively low spin bath of CaWO_4 , residual phonon populations and phonon-assisted processes remain relevant. Thus, deliberate strategies to suppress, redirect, or otherwise mitigate phonon participation is required to overcome the phonon bottleneck [36], rather than relying only on cryogenic cooling. One promising strategy is phononic engineering to modify the phonon dispersion of CaWO_4 .

For example, one approach is nanostructuring the host crystal to create phonon band gaps at selected eigen energies, particularly those chiefly responsible for causing

the loss of stored quantum states. In CaWO_4 , this includes suppressing or shifting the low-energy B_g mode at 9.1 meV to higher energies, where it is less thermally populated and less effective at coupling to Er^{3+} crystal-field levels. Such structures suppress the local phonon density of states, modify phonon dispersion, and reduce lattice-induced relaxation [36, 37, 55].

A complementary approach is to use phononic engineering to enhance heat extraction from the crystal [56, 57], which is especially important when substantial optical power is required to be applied during memory operation. For rare-earth-ion-doped systems, waveguides fabricated directly within the crystal can guide optical modes while allowing quantum states to propagate in regions where phonons are otherwise strongly suppressed, for example, near the natural 60–80 meV gap in CaWO_4 (Fig. 4). In such engineered environments, improved heat flow helps the crystal return to its base cryogenic temperature more rapidly, enabling higher repetition rates and the use of shorter, more intense optical control pulses without overheating.

V. CONCLUSION

In conclusion, we have mapped the phonon spectrum of CaWO_4 using inelastic neutron scattering and found excellent agreement with density-functional perturbation theory calculations. A symmetry analysis of the phonon eigenmodes identifies eight modes that can couple directly to Er^{3+} crystal-field levels and therefore play a central role in phonon-induced spin-lattice relax-

ation. Finally, we outlined phonon-engineering strategies to suppress or control these modes, providing pathways toward improving the photon storage times and performance of Er-doped CaWO_4 quantum memories.

VI. DATA AVAILABILITY

The data that support the findings of this study are available from the corresponding author upon reasonable request.

ACKNOWLEDGMENTS

The authors wish to thank N. Chilton, J. Bartholomew, R. Ahlefeldt, M. Sellars, J. and for helpful discussions. The proposal numbers for the data presented in this manuscript are #20241028 (EIGER, SINQ [40]), #19994 (Taipan, ANSTO [41, 42]). This research is supported by A*STAR under Project No. C230917009, Q.InC Strategic Research and Translational Thrust; the MTC Young Investigator Research Grant (Award # M24N8c0110); CQT++ Core Research Funding Grant (A*STAR). The authors would like to thank ACNS for the Taipan beamtime through proposal P19994. This work is based on experiments performed at the Swiss spallation neutron source SINQ, Paul Scherrer Institute, Villigen, Switzerland. Y. Z. and O. V. Y. acknowledge support by the Swiss National Science Foundation (grant 224624).

[1] Stephan Ritter, Christian Nölleke, Carolin Hahn, Andreas Reiserer, Andreas Neuzner, Manuel Uphoff, Martin Mücke, Eden Figueroa, Joerg Bochmann, and Gerhard Rempe. An elementary quantum network of single atoms in optical cavities. *Nature*, 484(7393):195–200, 2012.

[2] WL Yang, ZQ Yin, Y Hu, M Feng, and JF Du. High-fidelity quantum memory using nitrogen-vacancy center ensemble for hybrid quantum computation. *Physical Review A—Atomic, Molecular, and Optical Physics*, 84(1):010301, 2011.

[3] GD Fuchs, Guido Burkard, PV Klimov, and DD Awschalom. A quantum memory intrinsic to single nitrogen–vacancy centres in diamond. *Nature Physics*, 7(10):789–793, 2011.

[4] Olivier Pinel, Mahdi Hosseini, Ben M Sparkes, Jesse L Everett, Daniel Higginbottom, Geoff T Campbell, Ping Koy Lam, and Ben C Buchler. Gradient echo quantum memory in warm atomic vapor. *Journal of Visualized Experiments: JoVE*, (81):50552, 2013.

[5] Mahdi Hosseini, Geoff Campbell, Ben M Sparkes, Ping K Lam, and Ben C Buchler. Unconditional room-temperature quantum memory. *Nature Physics*, 7(10):794–798, 2011.

[6] YW Cho, GT Campbell, JL Everett, J Bernu, DB Higginbottom, MT Cao, J Geng, NP Robins, PK Lam, and BC Buchler. Highly efficient optical quantum memory with long coherence time in cold atoms. *Optica*, 3(1):100–107, 2016.

[7] Charles W Thiel, Thomas Böttger, and RL Cone. Rare-earth-doped materials for applications in quantum information storage and signal processing. *Journal of Luminescence*, 131(3):353–361, 2011.

[8] Manjin Zhong, Morgan P Hedges, Rose L Ahlefeldt, John G Bartholomew, Sarah E Beavan, Sven M Wittig, Jevon J Longdell, and Matthew J Sellars. Optically addressable nuclear spins in a solid with a six-hour coherence time. *Nature*, 517(7533):177–180, 2015.

[9] Yu Ma, You-Zhi Ma, Zong-Quan Zhou, Chuan-Feng Li, and Guang-Can Guo. One-hour coherent optical storage in an atomic frequency comb memory. *Nature Communications*, 12(1):2381, 2021.

[10] Fudong Wang, Miaomiao Ren, Weiye Sun, Mucheng Guo, Matthew J Sellars, Rose L Ahlefeldt, John G Bartholomew, Juan Yao, Shuping Liu, and Manjin Zhong. Nuclear spins in a solid exceeding 10-hour coherence times for ultra-long-term quantum storage. *PRX Quantum*, 6(1):010302, 2025.

[11] Yu-Ping Liu, Zhong-Wen Ou, Tian-Xiang Zhu, Ming-Xu Su, Chao Liu, Yong-Jian Han, Zong-Quan Zhou, Chuan-Feng Li, and Guang-Can Guo. A millisecond integrated quantum memory for photonic qubits. *Science Advances*, 11(13):eadu5264, 2025.

[12] Antonio Ortú, Adrian Holzäpfel, Jean Etesse, and Mikael Afzelius. Storage of photonic time-bin qubits for up to 20 ms in a rare-earth doped crystal. *npj Quantum Information*, 8(1):29, 2022.

[13] Khabat Heshami, Duncan G England, Peter C Humphreys, Philip J Bustard, Victor M Acosta, Joshua Nunn, and Benjamin J Sussman. Quantum memories: emerging applications and recent advances. *Journal of Modern Optics*, 63(20):2005–2028, 2016.

[14] WT Carnall, PR Fields, and K Rajnak. Electronic energy levels in the trivalent lanthanide aquo ions. I. Pr^{3+} , Nd^{3+} , Pm^{3+} , Sm^{3+} , Dy^{3+} , Ho^{3+} , Er^{3+} , and Tm^{3+} . *The Journal of Chemical Physics*, 49(10):4424–4442, 1968.

[15] K Matsuura, S Yasui, R Kaji, H Sasakura, T Tawara, and S Adachi. Exploration of optimal hyperfine transitions for spin-wave storage in $^{167}\text{Er}^{3+}:\text{Y}_2\text{SiO}_5$. *arXiv preprint arXiv:2412.10126*, 2024.

[16] D. L. McAuslan, J. G. Bartholomew, M. J. Sellars, and J. J. Longdell. Reducing decoherence in optical and spin transitions in rare-earth-metal-ion-doped materials. *Physical Review A*, 85:032339, 2012.

[17] Shi-Jia Wang, Yu-Hui Chen, Jevon J. Longdell, and Xiang-dong Zhang. Hyperfine states of erbium doped yttrium orthosilicate for long-coherence-time quantum memories. *Journal of Luminescence*, 262:119935, 2023.

[18] Miloš Rančić, Morgan P. Hedges, Rose L. Ahlefeldt, and Matthew J. Sellars. Coherence time of over a second in a telecom-compatible quantum memory storage material. *Nature Physics*, 14(1):50–54, January 2018.

[19] R Orbach. Spin-lattice relaxation in rare-earth salts. *Proceedings of the Royal Society of London. Series A. Mathematical and Physical Sciences*, 264(1319):458–484, 1961.

[20] GH Larson and CD Jeffries. Spin-lattice relaxation in some rare-earth salts. I. Temperature dependence. *Physical Review*, 141(1):461, 1966.

[21] Matteo Briganti, Fabio Santanni, Lorenzo Tesi, Federico Totti, Roberta Sessoli, and Alessandro Lunghi. A Complete Ab Initio View of Orbach and Raman Spin-Lattice Relaxation in a Dysprosium Coordination Compound. *Journal of the American Chemical Society*, 143(34):13633–13645, 2021. PMID: 34465096.

[22] Rangga P Budoyo, Kosuke Kakuyanagi, Hiraku Toida, Yuichiro Matsuzaki, William J Munro, Hiroshi Yamaguchi, and Shiro Saito. Phonon-bottlenecked spin relaxation of $\text{Er}^{3+}:\text{Y}_2\text{SiO}_5$ at sub-kelvin temperatures. *Applied Physics Express*, 11(4):043002, 2018.

[23] DA Garanin. Phonon bottleneck in the low-excitation limit. *Physical Review B—Condensed Matter and Materials Physics*, 77(2):024429, 2008.

[24] P Y Jia, X M Liu, G Z Li, M Yu, J Fang, and J Lin. Sol-gel synthesis and characterization of $\text{SiO}_2@\text{CaWO}_4,\text{SiO}_2@\text{CaWO}_4:\text{Eu}^{3+}/\text{Tb}^{3+}$ core-shell structured spherical particles. *Nanotechnology*, 17(3):734, 2006.

[25] R. F. Gonçalves, L. S. Cavalcante, I. C. Nogueira, E. Longo, M. J. Godinho, J. C. Sczancoski, V. R. Mastelaro, I. M. Pinatti, I. L. V. Rosa, and A. P. A. Marques. Rietveld refinement, cluster modelling, growth mechanism and photoluminescence properties of $\text{CaWO}_4:\text{Eu}^{3+}$ microcrystals. *CrystEngComm*, 17:1654–1666, 2015.

[26] LS Cavalcante, VM Longo, JC Sczancoski, MAP Almeida, AA Batista, José Arana Varela, Marcelo Ornaghi Orlandi, Elson Longo, and M Siu Li. Electronic structure, growth mechanism and photoluminescence of CaWO_4 crystals. *CrystEngComm*, 14(3):853–868, 2012.

[27] Malcolm Nicol and Jean F. Durana. Vibrational Raman Spectra of CaMoO_4 and CaWO_4 at High Pressures. *The Journal of Chemical Physics*, 54(4):1436–1440, 1971.

[28] T.T Basiev, A.A Sobol, Yu.K Voronko, and P.G Zverev. Spontaneous Raman spectroscopy of tungstate and molybdate crystals for Raman lasers. *Optical Materials*, 15(3):205–216, 2000.

[29] D. Christofilos, S. Ves, and G. A. Kourouklis. Pressure Induced Phase Transitions in Alkaline Earth Tungstates. *physica status solidi (b)*, 198(1):539–544, 1996.

[30] Yiguo Su, Guangshe Li, Yanfeng Xue, and Liping Li. Tunable physical properties of CaWO_4 nanocrystals via particle size control. *The Journal of Physical Chemistry C*, 111(18):6684–6689, 2007.

[31] Puneet Kaur, Atul Khanna, and Margit Fábián. Effects of annealing temperature on structural and photoluminescence properties of Eu, Dy and Sm doped CaWO_4 nanoparticles. *Ceramics International*, 46(17):27262–27274, 2020.

[32] Puneet Kaur, Atul Khanna, M.N. Singh, and A.K. Sinha. Structural and optical characterization of Eu and Dy doped CaWO_4 nanoparticles for white light emission. *Journal of Alloys and Compounds*, 834:154804, 2020.

[33] P.B. de Sousa, A.F. Gouveia, J.C. Sczancoski, I.C. Nogueira, E. Longo, M.A. San-Miguel, and L.S. Cavalcante. Electronic structure, optical and sonophotocatalytic properties of spindle-like CaWO_4 microcrystals synthesized by the sonochemical method. *Journal of Alloys and Compounds*, 855:157377, 2021.

[34] Prabhatasree Goel, MK Gupta, R Mittal, S Rols, SN Achary, AK Tyagi, and SL Chaplot. Inelastic Neutron Scattering Studies of Phonon Spectra and Simulations in Tungstates, AWO_4 ($\text{A} = \text{Ba}, \text{Sr}, \text{Ca}$ and Pb). *arXiv preprint arXiv:1407.6847*, 2014.

[35] K Kesavasamy and N Krishnamurthy. Phonon dispersions in calcium tungstate. *Canadian Journal of Physics*, 60(10):1447–1460, 1982.

[36] Jihong Ma. Phonon engineering of micro-and nanophononic crystals and acoustic metamaterials: a review. *Small Science*, 3(1):2200052, 2023.

[37] Thomas Lutz, Lucile Veissier, Charles W Thiel, Rufus L Cone, Paul E Barclay, and Wolfgang Tittel. Modification of phonon processes in nanostructured rare-earth-ion-doped crystals. *Physical Review A*, 94(1):013801, 2016.

[38] Michiel J Van Setten, Matteo Giantomassi, Eric Bousquet, Matthieu J Verstraete, Don R Hamann, Xavier Gonze, and G-M Rignanese. The pseudodojo: Training and grading a 85 element optimized norm-conserving pseudopotential table. *Computer Physics Communications*, 226:39–54, 2018.

[39] Hendrik J Monkhorst and James D Pack. Special points for brillouin-zone integrations. *Physical Review B*, 13(12):5188, 1976.

[40] U Stuhr, B Roessli, S Gvasaliya, HM Rønnow, U Filges, D Graf, A Bollhalder, D Hohl, R Bürge, M Schild, et al. The thermal triple-axis-spectrometer EIGER at the continuous spallation source SINQ. *Nuclear Instruments and Methods in Physics Research Section A: Accelerators, Spectrometers,*

Detectors and Associated Equipment, 853:16–19, 2017.

[41] SA Danilkin, Mohana Yethiraj, T Saerbeck, F Klose, C Ulrich, J Fujioka, S Miyasaka, Y Tokura, and B Keimer. TAIPAN: First results from the thermal triple-axis spectrometer at OPAL research reactor. In *Journal of Physics: Conference Series*, volume 340, page 012003. IOP Publishing, 2012.

[42] KC Rule, F Darmann, T Oste, D Bartlett, F Franceschini, A Berry, A McGregor, A Ogrin, T Ersez, A Kafes, et al. Recent enhancements and performance gains from upgrades to ANSTO’s thermal neutron instrument TAIPAN and the triple-axis and Be-filter spectrometers. *Nuclear Instruments and Methods in Physics Research Section A: Accelerators, Spectrometers, Detectors and Associated Equipment*, 901:140–149, 2018.

[43] Allan Zalkin and David H Templeton. X-ray diffraction refinement of the calcium tungstate structure. 1963.

[44] MI Kay, BC Frazer, and I Almodovar. Neutron diffraction refinement of CaWO_4 . *The Journal of Chemical Physics*, 40(2):504–506, 1964.

[45] Sean P Culver, Matthew J Greaney, Antonio Tinoco, and Richard L Brutchez. Low-temperature synthesis of homogeneous solid solutions of scheelite-structured $\text{Ca}_{1-x}\text{Sr}_x\text{WO}_4$ and $\text{Sr}_{1-x}\text{Ba}_x\text{WO}_4$ nanocrystals. *Dalton Transactions*, 44(33):15042–15048, 2015.

[46] Yi Yin, Yi-Ning Li, Sicheng Liu, Yan Jiang, Xiao-Yan Liu, and Peng Zhang. Theoretical study of efficient photon–phonon resonance absorption in the tungsten-related vibrational mode of scheelite. *ACS Omega*, 9(9):10517–10521, 2024.

[47] Yaoju Zhang, NAW Holzwarth, and RT Williams. Electronic band structures of the scheelite materials CaMoO_4 , CaWO_4 , PbMoO_4 , and PbWO_4 . *Physical Review B*, 57(20):12738, 1998.

[48] Zuocai Huang, Lei Zhang, Jing Feng, and Wei Pan. Physical properties of high-pressure scheelite YVO_4 from density functional calculations. *Computational Materials Science*, 69:527–532, 2013.

[49] Elrina Hartman, Michael E Tobar, Ben T McAllister, Jeremy F Bourhill, Andreas Erb, and Maxim Goryachev. Dielectric properties of single crystal calcium tungstate. *arXiv preprint arXiv:2507.21662*, 2025.

[50] A. Kinast, G. Angloher, S. Banik, G. Benato, A. Bento, A. Bertolini, R. Breier, C. Bucci, J. Burkhardt, L. Canonica, A. D’Addabbo, S. Di Lorenzo, L. Einfalt, A. Erb, F. v. Feilitzsch, N. Ferreiro Iachellini, S. Fichtinger, D. Fuchs, A. Fuss, A. Garai, V.M. Ghete, S. Gerster, P. Gorla, P.V. Guillaumon, S. Gupta, D. Hauff, M. Ješkovský, J. Jochum, M. Kaznacheeva, H. Kluck, H. Kraus, A. Langenkämper, M. Mancuso, L. Marini, L. Meyer, V. Mokina, A. Nilima, M. Olmi, T. Ortmann, C. Pagliarone, L. Pattavina, F. Petricca, W. Potzel, P. Povinec, F. Pröbst, F. Pucci, F. Reindl, J. Rothe, K. Schäffner, J. Schieck, D. Schmiedmayer, S. Schönert, C. Schwertner, M. Stahlberg, L. Stodolsky, C. Strandhagen, R. Strauss, I. Usherov, F. Wagner, M. Willers, V. Zema, F. Ferella, M. Laubenstein, and S. Nisi. Secular equilibrium assessment in a CaWO_4 target crystal from the dark matter experiment CRESST using Bayesian likelihood normalisation. *Applied Radiation and Isotopes*, 194:110670, 2023.

[52] Andreas Erb and Jean-Côme Lanfranchi. Growth of high-purity scintillating CaWO_4 single crystals for the low-temperature direct dark matter search experiments CRESST-II and EURECA. *CrystEngComm*, 15:2301–2304, 2013.

[53] R Strauss, G Angloher, A Bento, C Bucci, L Canonica, X Defay, A Erb, F von Feilitzsch, N Ferreiro Iachellini, P Gorla, A Gütlein, D Hauff, J Jochum, M Kiefer, H Kluck, H Kraus, J C Lanfranchi, J Loebell, A Münster, C Pagliarone, F Petricca, W Potzel, F Pröbst, F Reindl, K Schäffner, J Schieck, S Schönert, W Seidel, L Stodolsky, C Strandhagen, A Tanzke, H H Trinh Thi, C Türkoglu, M Ufflinger, A Ulrich, I Usherov, S Wawoczny, M Willers, M Wüstrich, and A Zöller. The CRESST-III low-mass WIMP detector. *Journal of Physics: Conference Series*, 718(4):042048, 2016.

[54] M Willers, G Angloher, A Bento, C Bucci, L Canonica, X Defay, A Erb, F v Feilitzsch, N Ferreiro Iachellini, A Gütlein, P Gorla, D Hauff, J Jochum, M Kiefer, H Kluck, H Kraus, J-C Lanfranchi, J Loebell, M Mancuso, A Münster, C Pagliarone, F Petricca, W Potzel, F Pröbst, R Puig, F Reindl, K Schäffner, J Schieck, S Schönert, W Seidel, M Stahlberg, L Stodolsky, C Strandhagen, R Strauss, A Tanzke, H H Trinh Thi, C Türkoglu, M Ufflinger, A Ulrich, I Usherov, S Wawoczny, M Wüstrich, and A Zöller. Direct dark matter search with the CRESST-III experiment - status and perspectives. *Journal of Physics: Conference Series*, 888(1):012209, sep 2017.

[55] L Eyring, Karl A Gschneidner, and GH Lander. *Handbook on the physics and chemistry of rare earths*, volume 32. Elsevier, 2002.

[56] Cleaven Chia, Bartholomeus Machielse, Benjamin Pingault, Michelle Chalupnik, Graham Joe, Eliza Cornell, Sophie Weiyi Ding, Stefan Bogdanović, Kazuhiro Kurouma, Afaq Habib Piracha, et al. Diamond quantum nanophotonics and optomechanics. In *Semiconductors and Semimetals*, volume 104, pages 219–251. Elsevier, 2021.

[57] Graham Joe, Cleaven Chia, Benjamin Pingault, Michael Haas, Michelle Chalupnik, Eliza Cornell, Kazuhiro Kurouma, Bartholomeus Machielse, Neil Sinclair, Srujan Meesala, et al. High Q-factor diamond optomechanical resonators with silicon vacancy centers at millikelvin temperatures. *Nano Letters*, 24(23):6831–6837, 2024.